Competing magnetic interactions in $La_{0.8}Y_{0.2}Mn_2Si_2$ - coexistence of canted ferromagnetism and antiferromagnetism

2000 J. Phys.: Condens. Matter 12 3241

(http://iopscience.iop.org/0953-8984/12/14/303)

J. Phys.: Condens. Matter **12** (2000) 3241–3254. Printed in the UK PII: S0953-8984(00)09493-5

Competing magnetic interactions in $La_{0.8}Y_{0.2}Mn_2Si_2$—coexistence of canted ferromagnetism and antiferromagnetism

M Hofmann†, S J Campbell‡‖ and S J Kennedy§

† Hahn–Meitner-Institut, BENSC, Glienickerstrasse 100, D-14109 Berlin, Germany
‡ School of Physics, University College, Australian Defence Force Academy, University of New South Wales, Canberra, ACT 2600, Australia
§ Neutron Scattering Group, ANSTO, Lucas Heights Research Laboratories, Menai, NSW 2234, Australia

E-mail: stewart.campbell@adfa.edu.au

Received 12 November 1999, in final form 8 February 2000

Abstract. The magnetic structures of tetragonal $La_{0.8}Y_{0.2}Mn_2Si_2$ have been investigated by neutron diffraction measurements over the temperature range ∼2–513 K. This compound corresponds to the critical concentration $x_c \sim 0.2$ in the $La_{1-x}Y_xMn_2Si_2$ series for the transition from the antiferromagnetism of YMn_2Si_2 to the predominant ferromagnetism of $LaMn_2Si_2$. The high temperature antiferromagnetic region of $La_{0.8}Y_{0.2}Mn_2Si_2$, $\sim 300\ \text{K} < T < T_{N1} \sim 410$ K, exhibits the planar antiferromagnetism common to the La-rich compounds in the $La_{1-x}Y_xMn_2Si_2$ series, with c-axis canted antiferromagnetic and ferromagnetic structures coexisting in the region $\sim 150\ \text{K} < T < T_{N2,C} \sim 300$ K. Below ∼150 K, $La_{0.8}Y_{0.2}Mn_2Si_2$ exhibits only the single phase canted antiferromagnetic structure. Rietveld refinements of the data demonstrate that the canted magnetic structures maintain the same angle of tilt with respect to the c-axis and the same total sublattice moment in the two phase region ∼150–300 K, and that the two tetragonal phases (both with the $ThCr_2Si_2$ structure) can be distinguished crystallographically with differences in their a lattice parameters and c lattice parameters of around $\Delta a \sim 0.012$ Å and $\Delta c \sim 0.007$ Å respectively. This simple description of these magnetic structures leads to a monotonic variation of the total Mn magnetic moment below $T_{N1} \sim 410$ K with the onset of the c-axis component occurring below $T_{N2,C} \sim 300$ K. The canted antiferromagnetic ground state of $La_{0.8}Y_{0.2}Mn_2Si_2$ can be described by the Mn moment values: $\mu_{Mn}(2\ \text{K}) = 2.25(4)\ \mu_B$, with the z-component of the moment $\mu_z(2\ \text{K}) = 1.87(4)\ \mu_B$, corresponding to a tilt angle $\theta(2\ \text{K}) = 33.7(9)^\circ$.

1. Introduction

Interest in the rare-earth intermetallics RT_2X_2 and related compounds (R = rare earth, T = transition metal, X = Si, Ge) of the tetragonal $ThCr_2Si_2$ structure (space group $I4/mmm$) has continued unabated in recent years (e.g. [1–3]). The RMn_2X_2 compounds are of particular interest as the Mn atoms carry a magnetic moment (e.g. [4–9]). The sensitive dependence of the magnetic behaviour and structures of these compounds on the Mn–Mn intraplanar distances and the interplanar separations (and correspondingly on the a-axis and c-axis lattice parameters respectively) leads to a wide range of magnetic behaviours and structures (e.g. [7, 10–12]). An understanding of the behaviour of this series of compounds has been extended significantly by the scope to investigate series of pseudo-ternary compounds in which either the rare-earth elements $(R, R')T_2X_2$ or the transition metal elements $R(T, T')_2X_2$ are varied, with interest in

‖ Corresponding author.

these compounds being further stimulated by recent studies which indicate the presence of a magnetic moment in transition metal atoms other than Mn [13].

Investigation of pseudo-ternary compounds such as $La_{1-x}Y_xMn_2Si_2$ are of particular interest as they allow the effects of competing magnetic interactions on the magnetic structures of the mixed compounds to be studied. As examples, the results of magnetic susceptibility and neutron diffraction measurements revealed ferromagnetic to antiferromagnetic transitions in $La_{1-x}Ce_xMn_2Si_2$ [10], $La_{1-x}Y_xMn_2Si_2$ [14, 15] and $La_{1-x}Y_xMn_2Ge_2$ [16] around critical concentrations of $x_c \sim 0.4$, ~ 0.2 and ~ 0.7 respectively. The complexity of the behaviour of these compounds is also revealed, for example, by the $La_{1-x}Y_xMn_2Si_2$ series for which spin-glass or cluster-glass-like behaviour is observed around $x_c \sim 0.2$ [14, 15]. A magnetic-field-induced antiferromagnetic to ferromagnetic transition has been observed for $La_{0.3}Y_{0.7}Mn_2Ge_2$ below 170 K [17] with changes in the hyperfine interaction parameters of $La_{1-x}Y_xMn_2Si_2$ (^{57}Fe) being observed around the critical concentration $x_c \sim 0.2$ [18]. Reflecting the extent of continuing interest in this type of compound, the effects of pressure on the magnetic behaviour of $La_{0.7}Y_{0.3}Mn_2Ge_2$ (120–370 K; 0–1.2 GPa [17]) and $Nd_{0.35}La_{0.65}Mn_2Si_2$ (150–440 K; 0–1.5 GPa; [19]) have been investigated.

Recently we reported the magnetic structures of this $La_{0.8}Y_{0.2}Mn_2Si_2$ sample based on a neutron diffraction study over the temperature range $\sim$4.2–450 K [20]. Ijjaali *et al* [21] obtained similar results in their investigation of the magnetic phase diagram ($\sim$2–500 K) of the $La_{1-x}Y_xMn_2Si_2$ solid solution using a combination of magnetic and neutron diffraction ($\sim$2–300 K) measurements. Here we present the results of an extended variable temperature neutron diffraction study ($\sim$2–513 K) of the critical compound $La_{0.8}Y_{0.2}Mn_2Si_2$. The results and analyses reveal the coexistence of both antiferromagnetic and ferromagnetic phases in $La_{0.8}Y_{0.2}Mn_2Si_2$ around the temperature region $\sim$150–300 K. A novel feature discovered for the system is that the optimal magnetic structures over this temperature region exhibit the same sublattice moment and tilt angle in both the ferromagnetic and antiferromagnetic phases, while exhibiting distinct crystallographic unit cells.

2. Experiment

Information on the standard method used for preparation of the sample has been given elsewhere [22]. In brief, the sample was prepared by standard arc melting in a partial pressure of purified argon (Mn 99.99%; La 99.99%; Y 99.99% and Si 99.7%). The starting materials contained $\sim$3% excess Mn to compensate for the Mn loss due to evaporation during melting and the ingot was melted five times for improved homogeneity. X-ray powder diffraction measurements established the presence of all of the reflections of the tetragonal $ThCr_2Si_2$ structure. Standard magnetic susceptibility measurements ($H = 100$ G) were carried out over the temperature range 4.2–350 K using a Quantum Technology SQUID magnetometer.

A comprehensive final set of neutron powder diffraction patterns was obtained over the temperature range 2–513 K on the diffractometer E6 at the Hahn–Meitner-Institut, Germany (wavelength $\lambda = 2.378$ Å), with earlier data having been obtained at ISIS, Rutherford Appleton Laboratory, UK and Reactor HIFAR, Lucas Heights Research Laboratories, Australia. The variable temperature experiments were carried out with the sample mounted in a standard cryofurnace. Rietveld refinements were carried out using the program packages GSAS [23] and FullProf [24] which allow simultaneous refinement of the structural and magnetic parameters. Using the coherent scattering lengths of $b_{La} = 8.24$ fm, $b_Y = 7.75$ fm, $b_{Mn} = -3.73$ fm and $b_{Si} = 4.15$ fm, and the Mn magnetic form factor given in [25], the parameters which were varied during the initial least square refinements included: a scale factor, four parameters for the background, the two lattice parameters and a positional parameter for the Si atom. In order to

account for preferred orientation effects we fitted an additional preferred orientation correction coefficient [26] to the data in the paramagnetic temperature region; this parameter was then fixed at this optimal value for all other temperatures. The isotropic thermal parameters and the Mn magnetic moment value were also refined.

3. Results and analysis

Figure 1 shows the neutron diffraction patterns obtained for the $La_{0.8}Y_{0.2}Mn_2Si_2$ compound over the temperature range 2–513 K. A Rietveld structure refinement using the powder diffraction data collected at 513 K confirmed that the sample crystallizes in the body centred tetragonal space group $I4/mmm$ as expected, with only trace levels (∼1%) of the LaMnSi phase present. The $ThCr_2Si_2$-type structure can be described as a stacking of atomic layers (each layer contains a single type of atom) along the crystallographic c-axis with the sequence –R–Si–Mn–Si–R–. In the ideal $ThCr_2Si_2$ structure the rare-earth and Si atoms occupy the Wyckoff positions 2(a) (0, 0, 0) and 4(c) (0, 0, z) with $z \sim 0.38$, while the Mn atoms are in the 4(d) sites at (1/2, 0, 1/4). The special position of the Mn atoms on the 4(d) sites means that nuclear scattering, and consequently scattering due to ferromagnetic ordering of the Mn atoms, contributes only to reflections obeying the (hkl) conditions $h + k = 2n$ and $l = 2n$ [4, 27].

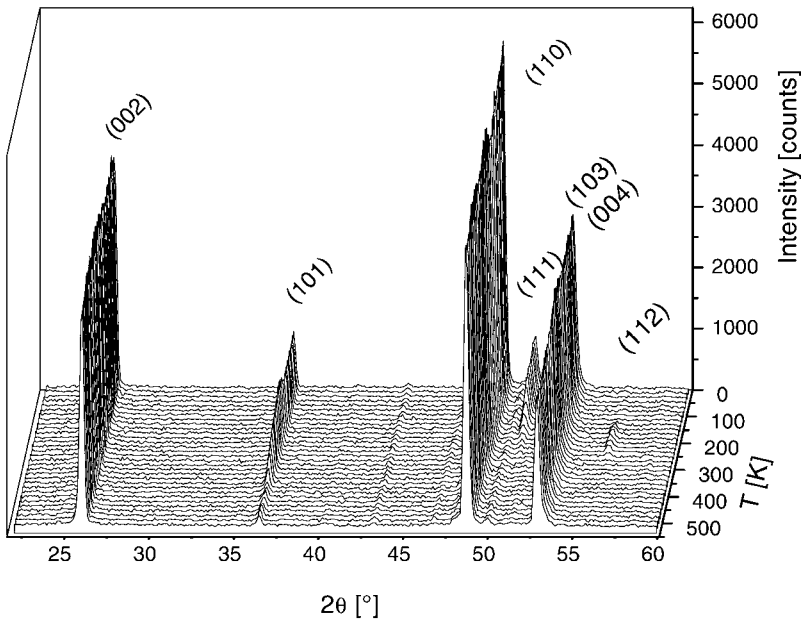

Figure 1. Neutron diffraction patterns of $La_{0.8}Y_{0.2}Mn_2Si_2$ from 513 K (bottom) to 2 K.

As noted in our earlier investigation [20], three distinct magnetic behaviours for the $La_{0.8}Y_{0.2}Mn_2Si_2$ compound can be readily distinguished as evidenced by the thermal evolution of the (101), (111) and (112) reflections. The increase in the intensity of the (101) reflection below $T_{N1} \sim 410$ K marks the onset of antiferromagnetic ordering within the (00l) Mn planes. As observed and discussed in relation to similar compounds such as $LaMn_2Si_2$ [4, 27], this antiferromagnetic contribution persists through the whole temperature region down to 2 K. In addition, the intensity ratio for the magnetic contributions of the (101) and (103)

peaks indicates that the moments lie in the (00l) plane rather than pointing along the c-axis. Below around 300 K additional magnetic superlattice reflections appear. These reflections can be indexed as (111), (113) and (201) on the basis of the chemical unit cell. The magnetic contribution to the intensity of these superlattice peaks, along with the absence of any (00l) reflections with $l = 2n+1$, is characteristic of the occurrence of ferromagnetic (00l) Mn planes which are coupled antiferromagnetically along the c-axis. In addition to these effects, figure 1 reveals clear evidence of a magnetic contribution to the (112) reflection over the temperature region ∼150–300 K. As described elsewhere [4, 20, 27], this contribution is associated with ferromagnetic ordering and, as no increases in intensities of the (00l) reflections with $l = 2n$ are observed, the ferromagnetic components of the moments are directed along the c-axis.

3.1. Rietveld refinements

The magnetic structures resulting from our refinements to the diffraction patterns (2–513 K) are shown in figure 2 (see also [20]). These structures are described using the notation developed by Venturini *et al* [28] for the magnetic ordering of the Mn sublattice in RMn_2X_2. The data were refined initially in the three temperature regimes as described below.

(i) $T_{N2,C} \sim 300\ K < T < T_{N1} \sim 410\ K$. The data were modelled using a planar antiferromagnetic G-type arrangement in the (00l) planes with a +− stacking along the c-axis similar to that already found for the high temperature magnetic phase in pure $LaMn_2Si_2$ and several other compounds (e.g. [4, 27]). Using the notation of Venturini *et al* [4, 28] this phase is denoted as AFl (see figure 2(a)).

(ii) $T <\sim 150\ K$. Since there is no ferromagnetic contribution to any peaks below ∼150 K and as only antiferromagnetic reflections of the type $h+k = 2n+1$ and $h+k+l = 2n+1$ are found, the refinements of the data were carried out using the AFmc type magnetic structure model. At 2 K this model leads to an antiferromagnetic moment value of $\mu_{Mn} = 2.25(4)\ \mu_B$ with a canting angle of $\theta \sim 33.7(9)^\circ$ relative to the c-axis.

(iii) $\sim 150\ K < T < T_{N2,C} \sim 300\ K$. The occurrence of ferromagnetic and antiferromagnetic features with an easy c-axis, as evidenced, for example, by the increased intensities in the (112) and (111) reflections in this region, indicates the presence of two magnetic structures. As discussed more fully below, this leads to the canted ferromagnetic and canted antiferromagnetic structures shown in figure 2(b) (labelled as Fmc) and figure 2(c) (AFmc) respectively.

The simultaneous appearance of ferromagnetic and antiferromagnetic ordering with moments oriented along an easy c-axis suggests a highly frustrated behaviour leading to the coexistence of two magnetic phases. Apart from this, further evidence for two *separate* phases in this temperature region can be found by inspection of the peak width of the (110) reflection. The d-spacings derived from this reflection give a direct measure for the intralayer Mn–Mn distance which is strongly correlated with the overall magnetic behaviour of RMn_2X_2 compounds, i.e. a transition from antiferromagnetism to ferromagnetism at $d_{crit} \sim 2.87$ Å [28]. Even though E6 is a medium resolution diffractometer, as shown in figure 3 a pronounced variation of the full width at half maximum (FWHM) of the (110) reflection (as determined by fitting to a Gaussian peak shape function) is observed over the temperature range where ferromagnetic and antiferromagnetic interactions occur. Given that outside this temperature range the peak width of the (110) reflection is close to the width expected from the instrumental resolution, the possibility that sample inhomogeneities are responsible for this broadening can be ruled out. In addition such inhomogeneities would be expected to contribute to broadening effects over the whole temperature region. The peak broadening could also be linked with

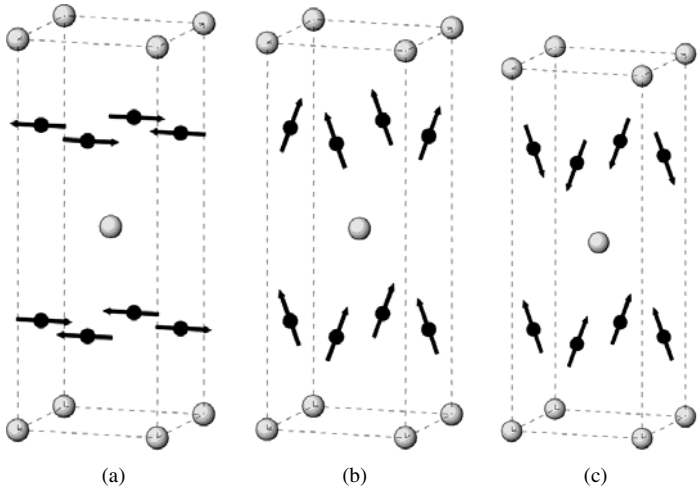

Figure 2. (a) The antiferromagnetic structure of $La_{0.8}Y_{0.2}Mn_2Si_2$ over the temperature range $T_{N2,C} \sim 300$ K $< T < T_{N1} \sim 410$ K (the Mn atoms are shown as small circles; for clarity the Si atoms are not shown). (b) The canted ferromagnetic structure of $La_{0.8}Y_{0.2}Mn_2Si_2$ over the temperature range ∼150–300 K. (c) The canted antiferromagnetic structure of $La_{0.8}Y_{0.2}Mn_2Si_2$ below $T_{N2,C} \sim 300$ K (this phase coexists with the canted ferromagnetic structure of figure 2(b) over the region ∼150–300 K) [20].

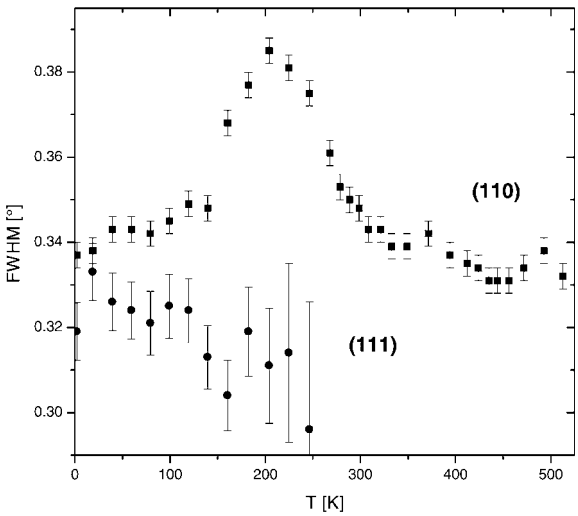

Figure 3. Thermal evolution of the full width at half maximum (FWHM) of the (110) (■) and (111) (●) peaks (the peaks were fitted using a Gaussian profile function).

microstrain or domain size effects. However inspection of the width of the purely magnetic (111) reflection from the AF*mc* phase shows an essentially constant value of around 0.32° over the temperature range 2–250 K (figure 3). This indicates negligible broadening due to sample effects and that the observed (110) broadening is due to the coexistence of two phases.

Apart from this pronounced broadening effect in the (110) reflection, there is a discrepancy in the peak positions of the (111) reflection as measured by standard peak fitting methods. This can be demonstrated by the a lattice parameter, c lattice parameter and d_{111}-spacing

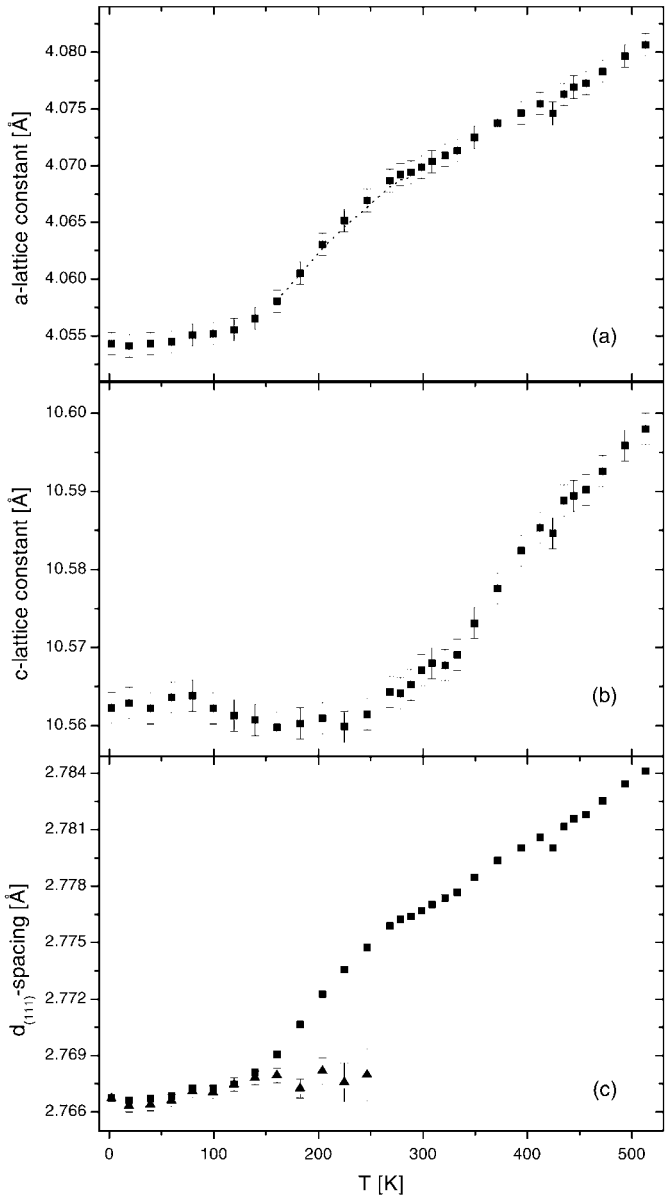

Figure 4. (a) Temperature dependence of the *a* lattice parameter and (b) temperature dependence of the *c* lattice parameter as determined by Rietveld refinements to the neutron diffraction patterns for $La_{0.8}Y_{0.2}Mn_2Si_2$ on the basis of a single phase (model A; the dashed line through the *a* lattice data in figure 4(a) is discussed in the text). (c) The d_{111}-values (■) calculated from the above *a* lattice parameters and *c* lattice parameters with the d_{111}-values obtained directly from the $2\theta_{111}$-reflections also shown (▲).

values, which are shown as a function of temperature in figures 4(a), 4(b) and 4(c) respectively. The *a* lattice parameter and *c* lattice parameter values (from which the d_{111}-values were then calculated) were determined from the refinements to the chemical unit cell of the diffraction patterns on the basis of a single phase only (i.e. with broadened reflections and temporarily

ignoring the above evidence for the presence of two phases). This refinement is labelled *model A*. Significant deviations of the expected trends of the a- and c-values established in the single phase regions are observed in the region ∼150–300 K. Figure 4 shows that the a lattice parameter rises sharply between ∼150 and 300 K, while the c lattice parameter, in agreement with the smaller linear compressibility observed in $LaMn_2Si_2$ [4], varies only slightly in this temperature region. The overall behaviours of the a lattice parameters and c lattice parameters are similar to those obtained by Ijjaali *et al* [21] over the temperature range ∼2–300 K. However of particular significance is to note the trend in the d_{111}-values (closed triangles in figure 4(c)) as determined directly from the diffraction patterns from the $2\theta_{111}$-values. This difference in behaviour between the two sets of d_{111}-values is further clear evidence in support of the coexistence of two phases as indicated above.

It should be noted that a monoclinic distortion around $T_{N2,C} \sim 300$ K could also account for the experimentally observed behaviours of the (110) peak widths (figure 3). However, the behaviour of the magnetic scattering excludes this possibility. Magnetic scattering is not observed for (002) reflections, thus excluding a ferromagnetic component in the plane as could be obtained for a monoclinic structure. Likewise, no magnetic scattering is obtained at (100) or (001) reflections as could be expected for an antiferromagnetic monoclinic structure. In addition, such a monoclinic distortion would require the unlikely combination of transitions from the tetragonal structure of the high temperature AFl phase to a monoclinic structure over the temperature range ∼150–300 K, before reverting from monoclinic back to the low temperature AFmc tetragonal structure below ∼150 K.

In light of the above, we conclude that a phase refinement approach using separate AFmc and Fmc phases rather than single-phase refinements is required to model correctly the magnetic behaviour of $La_{0.8}Y_{0.2}Mn_2Si_2$ in the temperature region from ∼150 to 300 K.

3.2. Rietveld refinements in the two-phase region (∼150–300 K)

Examples of the Rietveld refinements obtained for $La_{0.8}Y_{0.2}Mn_2Si_2$ over the temperature range 2–513 K and magnetic phases of interest are shown in figure 5. These refinements were obtained using *model B* and related analyses as outlined below. Summaries of the structural and magnetic parameters resulting from these refinements are given in table 1 with the temperature variation of the moment values shown in figure 6.

As strong correlations are expected between the scale factors and the moment values, and between the lattice constants of the two phases, several parameters had to be constrained during the refinements in the two-phase region. Attention was also paid to the behaviour of the antiferromagnetic moment of the AFmc phase in the temperature range $T \sim 150$–300 K as follows. Given that the temperature variation of the antiferromagnetic moment values in the AFmc phase can be determined for the single phase region for $T <\sim 150$ K, the moment values between $T \sim 150$ and 300 K were estimated using an empirical function to fit this set of refined low temperature data. The analysis was carried out using the expression $M(T) = M_0[1 - (T/T_N)^d]^e$ (where d and M_0 are fit parameters and e was fixed to the typical value of the critical exponent of the 3D Heisenberg ferromagnet 0.365 [29]) with the transition temperature T_N determined from the magnetic susceptibility results (see figure 8(b) as discussed below) as $T_{N2,C} = 300.9$ K. This expression was chosen as a convenient empirical function to represent the trends of the data, leading to the curve shown by the dotted line in figure 6. The moment values used in the refinements of the AFmc phase in the two-phase region were determined from the selected temperatures indicated by the open triangles in figure 6, with the closed triangles representing the refined moment values determined for the single AFmc phase for $T < 150$ K. The lattice parameters for the antiferromagnetic phase in the

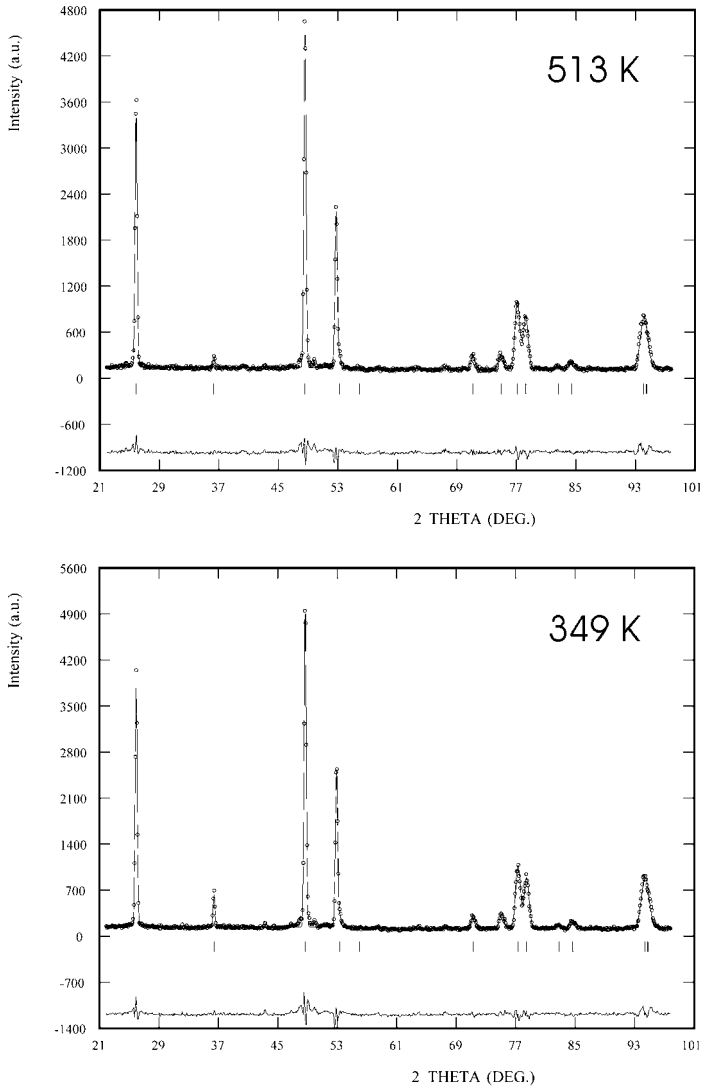

Figure 5. Plots of Rietveld refinements based on the two-phase model B (see text) to the diffraction patterns at the temperatures indicated along with phase markers: 513 K, 349 K, 246 K (F*mc* (top), AF*mc* (bottom)), 2 K.

two-phase region were derived by linear extrapolation of the lattice constants refined from the data in the single-phase region below 150 K. All other parameters were varied as for the data sets refined for $T > 300$ K and $T < 150$ K.

The temperature variations of the lattice parameters and phase fractions as determined from the refinements and related analyses are shown in figures 7(a) and 7(b) respectively (the slight shift in the refined F*mc* *a* lattice parameter values around 280 K of ∼0.002 Å is an artefact which stems from the choice of extrapolated values from the AF*mc* phase and is linked with the onset of the two phases and the limited resolution). The dashed line in figure 7(a) (also reproduced in figure 4(a)) represents the mean *a* lattice parameter values obtained by weighting the AF*mc* and F*mc* lattice parameters by their phase fractions (figure 7(b)); these

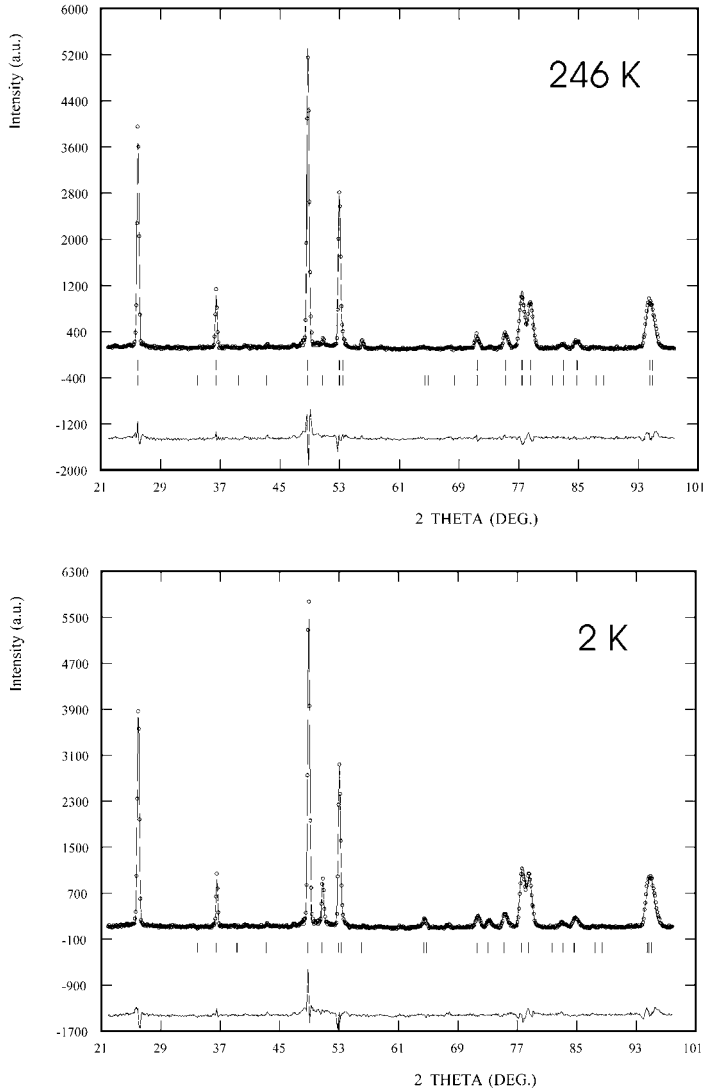

Figure 5. (Continued)

values are found to be in excellent agreement with the *a* lattice parameter values obtained from the simplified analysis in terms of the single-phase model A. However, as discussed below, a minor but significant modification to the refinements in which the total moment and tilt angles values of the ferromagnetic and antiferromagnetic phases are constrained to be the same (*model B′*), leads to the improved, final description of the moment values shown in figure 8(a).

4. Discussion and conclusions

Insight into the complex magnetic behaviour exhibited by $La_{0.8}Y_{0.2}Mn_2Si_2$ stems from the unequivocal identification of the two-phase region. As noted above there are several experimental features which point to the coexistence of two phases in the temperature region

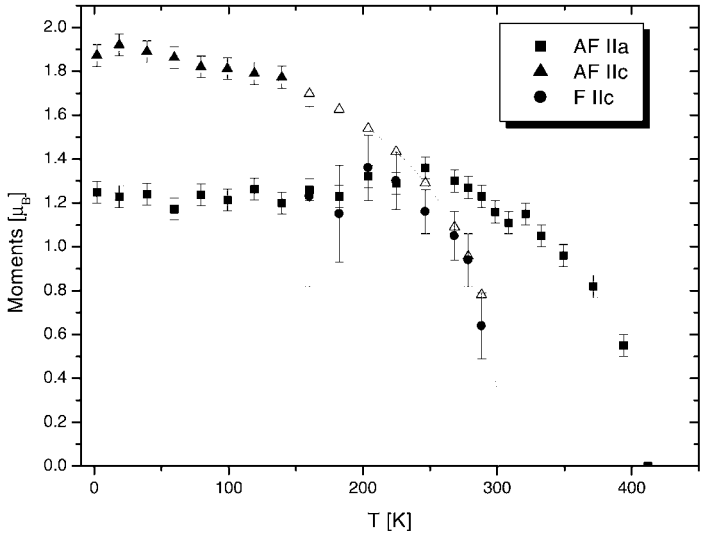

Figure 6. The temperature dependence of the components of the Mn moment values as determined from the Rietveld refinements (model B; see text) to the neutron diffraction patterns of figure 1. As discussed in the text, the full line represents the function $M(T) = M_0[1 - (T/T_N)^d]^e$ with $M_0 = 1.89(1)\ \mu_B$, $d = 2.2(2)$, $e = 0.365$ and $T_N = 300.9$ K. The open triangles represent analytical values for the AF*mc* moment in the two-phase region with the refined values (determined from the diffraction patterns for $T < 150$ K) shown as closed triangles. Note that the final moment values for $La_{0.8}Y_{0.2}Mn_2Si_2$ are presented in figure 8 (model B′; see text).

Table 1. Structural and magnetic parameters of $La_{0.8}Y_{0.2}Mn_2Si_2$ as determined from Rietveld refinements of neutron diffraction patterns at the temperatures indicated (cf figure 1). The refinements were obtained using the two-phase model B over the temperature range ∼150–300 K as discussed in the text. The refinement of the 246 K neutron diffraction pattern resulted in the two sets of lattice parameter values shown below.

Parameter	513 K	349 K	246 K	2 K
a [Å]	4.0810(9)	4.0729(9)	4.0556(9)	4.0540(9)
c [Å]	10.597(2)	10.571 (2)	10.557(2)	10.556(2)
a (II) [Å]	—	—	4.0687(9)	—
b (II) [Å]	—	—	10.550(3)	—
z (Si)	0.3819(7)	0.3808(6)	0.3801(7)	0.3799(8)
μ_x [μ_B]	—	0.95(5)	1.36(5)	1.25(4)
μ_z (AF/F) [μ_B]	—	—	1.30(5)	1.87(4)
μ_{tot} [μ_B]	—	0.95(5)	1.89(5)	2.25(4)
Canting angle [°]	—	90	46.4(17)	33.7(9)
R_{wp} [%]	12.0	12.9	14.3	14.8
R_{Bragg} [%]	5.7	5.9	6.1	7.5
R_{mag} [%]	—	3.9	4.5	6.4

∼150–300 K that are distinct both crystallographically and magnetically. These include: the broadening of the (110) reflections (and the (200) reflections as measured by separate x-ray diffraction experiments [30]), yet the absence of broadening in the purely magnetic (111) peak (figure 3); the steep slope in the a lattice parameter (figure 4(a)) and the minimum in the c lattice parameter (figure 4(b)). In addition the d-spacings of the (111) antiferromagnetic peaks do not follow those calculated from the lattice parameters derived from single-phase refinements, but extrapolate well from the low temperature single-phase region.

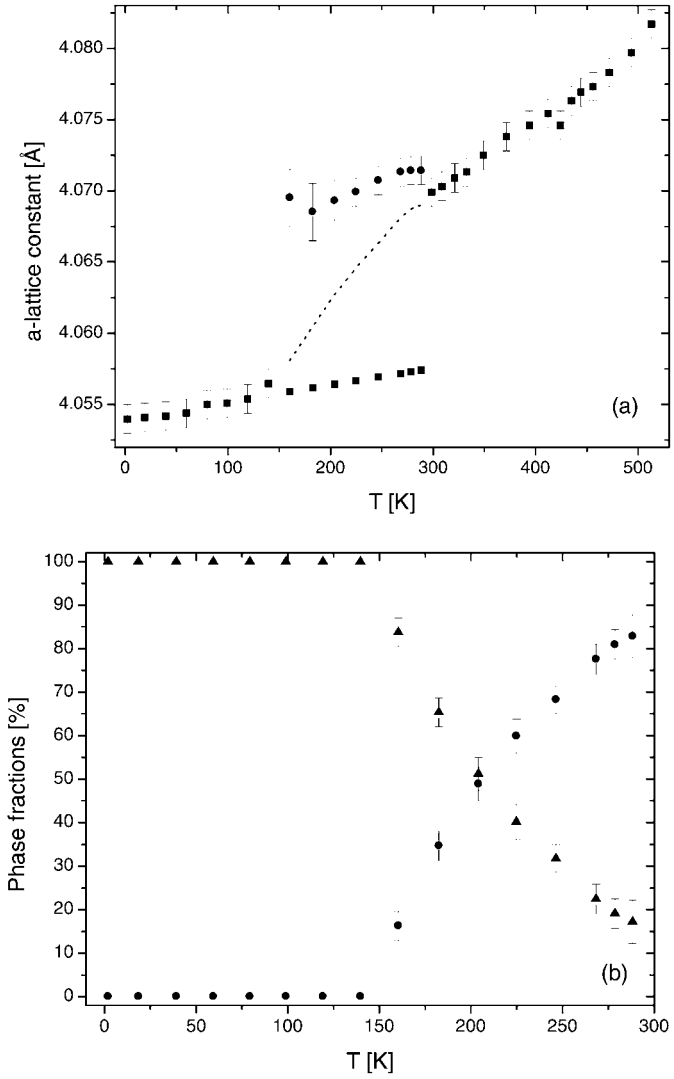

Figure 7. (a) The *a* lattice parameters as determined from Rietveld refinements (two-phase model B as discussed in the text) to the neutron diffraction patterns of figure 1. The dashed line (also reproduced in figure 4(a)) shows the weighted lattice parameters obtained by linear combination (weighted by the phase fractions; figure 7(b)) of the *a*-lattice parameters for the two phases in the temperature region ∼150–300 K. (b) Fractions of the AF*mc* (▲) and F*mc* phases (●) present in $La_{0.8}Y_{0.2}Mn_2Si_2$ as determined from the refinements.

The simplest interpretation of these observations is one in which we ascribe the low temperature antiferromagnetic AF*mc* structure (figure 2(c)) to the smaller cell in which the *a* lattice parameter is reduced and in which the *c* lattice parameter is slightly increased. If we then ascribe the higher temperature F*mc* phase to the ferromagnetic coupling (figure 2(b)), in which the *a* lattice parameter is increased and the *c* lattice parameter is slightly reduced, we see that this agrees well with all of the observations listed above. On cooling from the high temperature, planar antiferromagnetic phase ($T > 300$ K), the *a* lattice parameter reaches a critical value (corresponding to an intraplanar Mn–Mn distance of 2.876(1) Å) where the moments begin

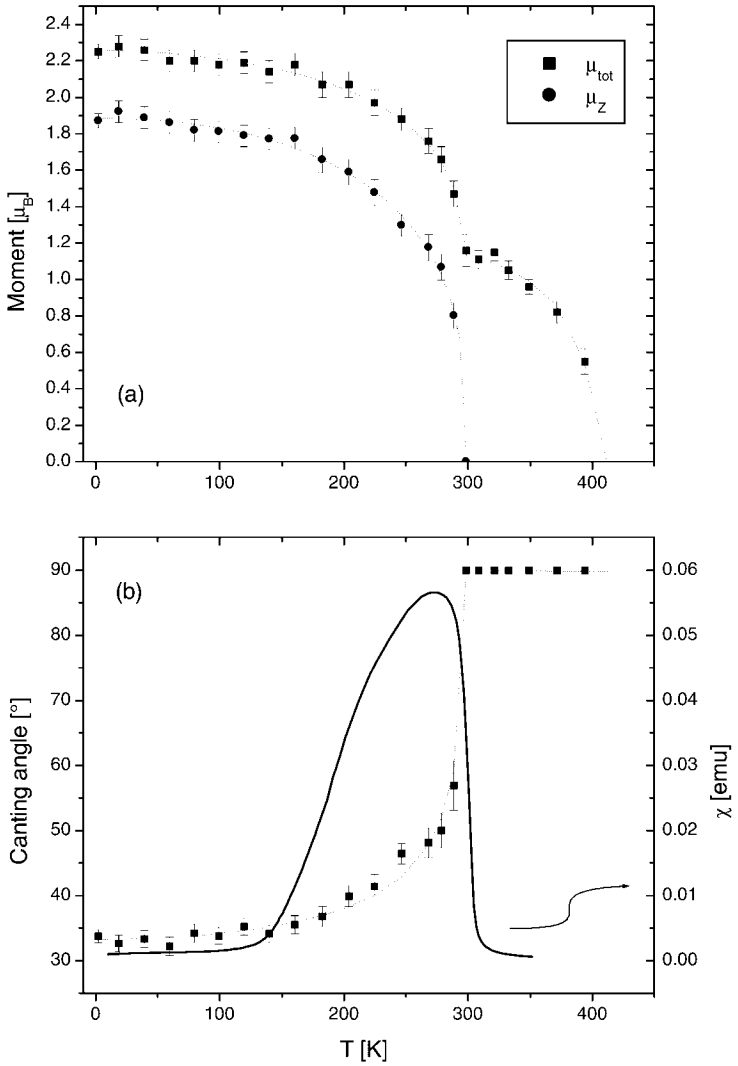

Figure 8. (a) The total Mn magnetic moment and μ_z values for $La_{0.8}Y_{0.2}Mn_2Si_2$ as a function of temperature below $T_{N1} \sim 410$ K. The moment values were obtained by Rietveld refinements based on the two-phase model B′ with equal canting angle for the two magnetic phases, F*mc* and AF*mc*, below $T_{N2,C} \sim 300$ K. (b) The canting angle θ relative to the *c*-axis, for the Mn magnetic moment in the F*mc* and AF*mc* phases. The DC magnetic susceptibility curve ($H = 100$ G) for $La_{0.8}Y_{0.2}Mn_2Si_2$ is shown as a full line. The dotted lines in figures 8(a) and 8(b) act as guides to the eye.

to cant towards the *c*-axis. Initially this takes the form of ferromagnetic coupling between axial components leading to the magnetic structure F*mc* (figure 2(b)) but, as the cell contracts further, the interplanar exchange reverts to antiferromagnetic coupling (AF*mc*, figure 2(c)). That there is such a broad overlap between the two phases suggests that this compound crosses the critical distance gradually. This leads us to conclude that the critical parameter which drives this phase change is the *c*-axis interplanar distance 5.278(2) Å. The anomaly in the *a* lattice parameters comes about through magneto-elastic coupling so that, as the interplanar exchange

reverts from ferromagnetic to antiferromagnetic, there is a contraction of the a lattice parameter by ∼0.3%. Figure 4(b) suggests that this is accompanied by a small but visible expansion of the c-axis (∼0.06%). High resolution diffraction measurements are required to confirm and quantify such slight changes in the c-axis lattice parameter (these measurements would also allow the relatively small 2θ range available from the relatively long wavelength, $\lambda = 2.378$ Å, of the E6 diffractometer to be extended).

A simple extension to this magnetic model provides a further test of this interpretation as follows. We assume in the final two-phase model B′ that the phases have *the same magnetic moment magnitude and the same angle of tilt with respect to the c-axis*. The only difference, apart from the lattice parameter values, is that the interplanar coupling is ferromagnetic in the larger cell and antiferromagnetic in the smaller cell. (It should be noted, however, that these final refinements were carried out with a fixed difference between the Fmc and AFmc phases for the a lattice parameters of $\Delta a = +0.0115$ Å and between the c lattice parameters of $\Delta c = -0.007$ Å respectively. It was necessary to constrain the differences in a and c because the resolution of the measurement was insufficient to resolve the relevant diffraction peaks.) The Rietveld refinements confirm that this final model B′ gives superior fits to those obtained using a common unit cell to describe each of the ferromagnetic and antiferromagnetic features independently as used in model A. This explanation of the correlation of the sign of the magnetic exchange coupling with critical values of intraplanar and interplanar distances is consistent with the earlier behaviour reported for RMn_2X_2 compounds [10].

The essential simplicity of this modified two-phase model B′ in accounting for the complex magnetic behaviour exhibited by $La_{0.8}Y_{0.2}Mn_2Si_2$ is epitomized in figure 8(a) which shows a graph of the total Mn moment as a function of temperature below $T_{N_1} \sim 410$ K. As expected, the variation of the total magnetic moment with temperature is similar to that exhibited by the magnetic hyperfine field of ^{57}Fe doped $La_{0.8}Y_{0.2}Mn_2Si_2$ as determined by Mössbauer effect studies [31]. Likewise, the variation of the magnetic hyperfine field of other ^{57}Fe doped La-rich compounds ($x < 0.25$) in the $La_{1-x}Y_xMn_2Si_2$ series, reveals magnetic transitions which agree with the magnetic structural transitions determined by neutron diffraction [31]. Also shown in figure 8(a) is μ_z, the z-component of the moment, which occurs with onset of spin canting below $T_{N2,C} \sim 300$ K, and the tilt angle θ relative to the c-axis (figure 8(b)). The equivalence of the tilt angle in the ferromagnetic Fmc and antiferromagnetic AFmc phases leads to the regular variation of μ_z with temperature as expected below the magnetic transition temperature $T_{N2,C} \sim 300$ K. By comparison, refinements to the data based on the two-phase model B (but lacking the equal tilt angle below $T_{N2,C}$), leads to the complex variations of the components of the Mn moments represented in figure 6. The magnetic susceptibility curve obtained in the SQUID magnetometer (figure 8(b)) reflects primarily the behaviour of the ferromagnetic Fmc region over the temperature range ∼150–300 K. A sharp rise in magnetization is observed at $T_{N2,C} \sim 300$ K with the gradual decrease in magnetic susceptibility taking place as the lattice contracts and the antiferromagnetic AFmc phase develops at the expense of the ferromagnetic Fmc phase (figure 7(b)).

In conclusion, the complex magnetic behaviour exhibited by $La_{0.8}Y_{0.2}Mn_2Si_2$ which experiences competing ferromagnetic and antiferromagnetic interactions, leads to the magnetic structures shown in figure 2 as determined by neutron diffraction measurements over the temperature regions indicated (see also [20, 21]). The optimal structural models for the Fmc and AFmc structures, which have been shown to coexist over the temperature region ∼150–300 K, are obtained with the same tilt angle for these canted ferromagnetic and antiferromagnetic structures. This commonality in behaviour between related magnetically canted phases is likely to occur in other RMn_2X_2 compounds with the tetragonal $ThCr_2Si_2$ structure, leading to simplifications in their phase diagrams. This is evidenced by comparisons between the

magnetic moment behaviour of $La_{0.8}Y_{0.2}Mn_2Si_2$ as determined using the correct model B′ (figure 8) and that obtained for model B (figure 6). The ground state for $La_{0.8}Y_{0.2}Mn_2Si_2$ is a canted antiferromagnet (AFmc) of Mn magnetic moment value at 2 K of $\mu_{Mn} = 2.25(4)\ \mu_B$, with the z-component of the moment $\mu_Z = 1.87(4)\ \mu_B$, corresponding to a canting angle $\theta = 33.7(9)^\circ$.

Acknowledgments

This work was supported in part by a grant from the Australian Research Council. We acknowledge access to the LAD and POLARIS diffractometers at the ISIS Facility, Rutherford Appleton Laboratory, UK, and thank the instrument scientists Dr W S Howells and Dr R Smith for their assistance. This work was also supported by the Access to Major Research Facilities Program, ANSTO, Lucas Heights Research Laboratories, Australia, and the Australian Institute of Nuclear Science and Engineering.

References

[1] Szytula A and Leciejewicz J 1994 *Handbook of Crystal Structures and Magnetic Properties of Rare Earth Intermetallics* (Boca Raton, FL: Chemical Rubber Company)
[2] Venturini G and Malaman B 1996 *J. Alloys Compounds* **235** 201
[3] Norlidah N M, Venturini G and Malaman B 1998 *J. Alloys Compounds* **268** 29
[4] Venturini G, Welter R, Ressouche E and Malaman B 1994 *J. Alloys Compounds* **210** 213
[5] Nowik I, Lavi Y, Felner I and Bauminger E R 1995 *J. Magn. Magn. Mater.* **147** 373
[6] Wada H, Yamaguchi H and Shiga M 1996 *J. Magn. Magn. Mater.* **152** 165
[7] Venturini G 1996 *J. Alloys Compounds* **232** 133
[8] Xi H, Liang G, Mochizuki K, Tang B and Markert J T 1997 *J. Magn. Magn. Mater.* **175** 319
[9] Sokolov A, Wada H, Shiga M and Goto T 1998 *Solid State Commun.* **105** 289
[10] Sytula A and Siek S 1982 *J. Magn. Magn. Mater.* **27** 49
[11] Brabers J H V J, Nolten A J, Kayzel F, Lenczowski S H J, Buschow K H J and de Boer F R 1994 *Phys. Rev.* B **50** 16 410
[12] Venturini G, Malaman B and Ressouche E 1996 *J. Alloys Compounds* **237** 61
[13] Ijjaali I, Venturini G and Malaman B 1999 *J. Alloys Compounds* **284** 10
[14] Chaughule R S, Radhakrishnamurty C, Sampathkumaran E V, Malik S K and Vijayaraghavan R 1983 *Mater. Res. Bull.* **18** 817
[15] Sampathkumaran E V, Chaughule R S, Gopalakrishnan K V, Malik S K and Vijayaraghavan R 1983 *J. Less-Common Met.* **92** 35
[16] Fujii H, Inoda M, Okamoto T, Shigeoka T and Iwata N 1986 *J. Magn. Magn. Mater.* **54–57** 1345
[17] Kaneka T, Kanomata T, Yasui H, Shigeoka T, Iwata M and Nakagawa Y 1992 *J. Phys. Soc. Japan* **61** 4164
[18] Li Hong-Shuo, Cadogan J M, Zhao X L and Campbell S J 1995 *J. Magn. Magn. Mater.* **147** 91
[19] Duraj R, Szytula A, Malaman B and Venturini G 1999 *J. Magn. Magn. Mater.* **192** 481
[20] Hofmann M, Campbell S J, Smith R I, Kennedy S J, Zhao X L and Edge A V J 1998 *Mater. Sci. Forum* **278–281** 553
[21] Ijjaali I, Venturini G, Malaman B and Ressouche E 1998 *J. Alloys Compounds* **266** 61
[22] Hofmann M, Campbell S J, Zhao X L, Li H S and Cywinski R 1996 *Mater. Sci. Forum* **228–231** 587
[23] Larson A C and Von Dreele R B 1994 LAUR 86-748, LANCSE MS-H805, Los Alamos National Laboratory
[24] Rodriguez-Carvajal J 1998 *FullProf* version 3.5, LLB
[25] Hahn T (ed) 1992 *International Tables for Crystallography* vol C (Dordrecht: Reidel)
[26] Dollase W A 1986 *J. Appl. Crystallogr.* **19** 267
[27] Hofmann M, Campbell S J, Kennedy S J and Zhao X L 1997 *J. Magn. Magn. Mater.* **176** 279
[28] Venturini G, Welter R, Ressouche E and Malaman B 1995 *J. Magn. Magn. Mater.* **150** 197
[29] Hagdorn K, Hohlwein D, Ihringer J, Knorr K, Prandl W, Ritter H, Schmid H and Zeiske Th 1999 *Eur. Phys. J.* B **11** 243
[30] Hofmann M, Campbell S J *et al* 2000 in preparation
[31] Campbell S J, Cadogan J M, Zhao X L, Hofmann M and Li Hong-Shuo 1999 *J. Phys.: Condens. Matter* **11** 7835